The Human Amyloid Precursor Protein Binds Copper Ions with Dominant Picomolar Affinity via the Helix-Rich E2 Domain

Tessa R. Young,[a] Tara L Pukala,[b] Roberto Cappai,[c] Anthony G. Wedd [a] and Zhiguang Xiao*[a,d]

[a] School of Chemistry and Bio21 Molecular Science and Biotechnology Institute, The University of Melbourne, Parkville, Victoria 3010, Australia

[b] Discipline of Chemistry, The University of Adelaide, Adelaide, SA 5005, Australia

[c] Department of Pharmacology and Therapeutics, The University of Melbourne, Parkville, Victoria, 3010, Australia.

[d] Melbourne Dementia Research Centre, Florey Institute of Neuroscience and Mental Health, The University of Melbourne, Parkville, Victoria, 3052, Australia.

* zhiguang.xiao@florey.edu.au

Electronic Supplementary Information

EXPERIMENTAL PROCEDURES

1. Materials and general methods

Reagents including buffers (Mops, Mes, Ches), ligands (Fs, Fz, Bca, Bcs), metal salts ($CuSO_4$•5(H_2O), $Cu(OAc)_2$•(H_2O), reductants (NH_2OH, Asc) and heparin (H3393, from porcine intestinal mucosa) were purchased from Sigma-Aldrich and were used as received. Heparin concentrations were estimated by mass, assuming an average molar mass of 19 kDa for the H3393 mixture.[1] Cu(II) standards were prepared by dissolving cupric salts in Milli-Q water. Their concentrations were calibrated via reaction with excess ligand Bcs in MOPS buffer containing reductant NH_2OH. Under such conditions, copper ions are converted quantitatively to the chromophore $[Cu^{I}(Bcs)_2]^{3-}$ (λ_{max}, 483 nm; $\varepsilon = 13{,}000\ M^{-1}\ cm^{-1}$).[2] Peptide probes (DP1-3) were custom synthesised by GL Biochem (Shanghai), using Fmoc-L-Lys(dansyl)-OH to supply the dansyl moiety at the ε-amino group of the sole lysine residue in each peptide sequence. The identity and purity (> 98%) of each peptide was confirmed by electrospray ionisation mass spectrometry (ESI-MS) and HPLC, and concentrations determined spectroscopically (λ_{max} ~ 326 nm; $\varepsilon = 4500\ M^{-1}\ cm^{-1}$). Human serum albumin (HSA) was purchased from Sigma Aldrich as a lyophilised powder. Its purity was confirmed by SDS-PAGE and spectroscopy (λ_{max} ~ 280 nm; $\varepsilon = 34{,}445\ M^{-1}\ cm^{-1}$).

The protein domains and their Cu(II)-complexes tended to precipitate in neutral buffer solutions but increased ionic strength via NaCl, enhanced solubility. In competition experiments, a standard NaCl concentration (100 mM) was used. In cases where high concentrations of protein were required, the concentration of NaCl was adjusted accordingly, as indicated in the text.

2. Expression and purification of APP E2 domain from *Escherichia coli*

Protein domains APP E2 (residues 295-498 of APP_{695}) and E2-qm (a quadruple mutant with the four His residues of the M1 site converted to Ala: H313,382,432,436A) were expressed in *Escherichia coli* BL21(DE3) cells and purified as reported.[3] These were generated in their N-terminal acetylated forms by co-expression of a NatB acetylation complex, as previously described.[3,4]

3. Expression of APP domains D1, D2, E1 and sAPPα from *Pichia pastoris*

The complete extracellular domain sAPPα (residues 18-611) of APP and the separate subdomains D1 (28-123), D2 (133-189) and E1 (28-189) were expressed and purified from *Pichia pastoris* cells according to published procedures.[5-8] The *Pichia pastoris* cells transformed with the respective expression plasmids were grown for ~ 48 hrs in YPD media in shaking flasks (30 °C, 150 rpm). Cells were then pelleted and protein expression induced by resuspending the harvested cells in induction (YPM) media and incubating cultures (30 °C, 150 rpm) for 48 – 72 hrs. Cultures were then centrifuged (3000 g, 30 mins, 4 °C) and the supernatant, containing the secreted recombinant protein target, was collected and filtered through a 0.2 μm membrane. Protein purification was conducted using a variation on previously described methods,[5,9] as outlined below.

4. Purification of APP domains D1, D2, E1

Culture supernatant in buffer solution (20 mM sodium phosphate, pH 7.4, 500 mM NaCl, 10 mg/L PMSF) was loaded onto a Cu(II)-NTA resin, washed with 10 CVs high-salt buffer (20 mM sodium phosphate, pH 7.4, 500 mM NaCl) and eluted with imidazole solution (20 mM sodium phosphate, pH 7.4, 500 mM NaCl, 250 mM imidazole). Elution fractions were purified by size-exclusion chromatography using a Superdex 75 HiLoad 16/60 column (GE Healthcare) in Mops buffer (20 mM,

pH 7.4, 100 mM NaCl). For domains D1 and D2 only, an additional hydrophobic interaction chromatography (HIC) step was required. Protein fractions were diluted with an equal volume of binding buffer (50 mM sodium phosphate, pH 7.0, 2.0 M $(NH_4)_2SO_4$) and loaded to a HiLoad 16/10 phenyl sepharose column (GE Healthcare). The column was washed with buffer (50 mM sodium phosphate, pH 7.0, 1.0 M $(NH_4)_2SO_4$) and eluted with a linear $(NH_4)_2SO_4$ gradient (1.0 – 0 M). Collected fractions were concentrated and buffer exchanged (20 mM Mops, pH 7.4, 100 mM NaCl) using centrifugal filters and stored at –80 °C.

5. Purification of full length sAPPα

Culture supernatant in buffer solution (20 mM L-histidine, pH 5.7, 50 mM EDTA, 10 mg/L PMSF) was loaded onto a DE-52 anion exchange resin (Whatman), washed with 10 CVs wash buffer (20 mM L-His, 5 mM EDTA, 150 mM NaCl, 10 mg/L PMSF) and eluted with a linear (150 – 800 mM) NaCl gradient. Protein-containing elution fractions were diluted with an equal volume of binding buffer (50 mM sodium phosphate, pH 7.0, 2.0 M $(NH_4)_2SO_4$) and loaded onto a HiLoad 16/10 phenyl sepharose column (GE Healthcare). The column was washed with buffer (50 mM sodium phosphate, pH 7.0, 1.0 M $(NH_4)_2SO_4$) and eluted with a linear $(NH_4)_2SO_4$ gradient (1.0 – 0 M). Elution fractions separated into sAPPα and a truncated fragment (sAPPα-tr), which were each separately purified by size-exclusion chromatography on a Superdex 200 10/300 GL column (GE Heathcare) in Mops buffer (20 mM, pH 7.4, 100 mM NaCl). Collected fractions were concentrated using centrifugal filters and stored at –80 °C. Protein purity was confirmed by SDS-PAGE and UV-visible spectroscopy. The latter was used to confirm the removal of highly-absorbing media contaminants from *Pichia* supernatants. The spectra of purified samples showed a single peak centred at 280 nm, and an absorbance ratio of $A_{260} : A_{280} \sim 0.6$ characteristic of the purified protein (see Figures S1b, S2).

6. Protein identification and quantification

The identity of each purified APP protein domain was confirmed by ESI-MS analysis (Table 1). The single exception is sAPPα whose identity was confirmed by in-gel trypsin digestion (with in-gel reduction-alkylation steps) and LC-MS peptide mapping (Figures S3, S4), following reported protocols.[10] The details are given in section 7 below.

Protein concentrations were estimated based on solution absorbance at 280 nm using molar extinction coefficients calculated from their respective amino acid compositions assuming all cysteines form disulfide bonds: ε = 15,930 cm^{-1} M^{-1} for E2 proteins; 15,845 cm^{-1} M^{-1} for D1; 7,365 cm^{-1} M^{-1} for D2; 23,210 cm^{-1} M^{-1} for E1; and 60,110 cm^{-1} M^{-1} for sAPPα.

7. Identification and characterisation of sAPPα

sAPPα was expressed in the methylotrophic yeast *Pichia pastoris* and isolated as two major protein species: (i) the full-length sAPPα ectodomain and (ii) a smaller truncated species (sAPPα-tr), presumably derived from partial degradation of the full length protein during isolation (Figure S1a), as reported previously[5]. The two species were isolated and characterised separately. Spectroscopic data (Figure S1b) indicated a high purity of both samples.

A high degree of heterogeneity from PTMs prevented sequence identification from high-resolution ESI-MS. Instead, samples of both the sAPPα and sAPPα-tr were excised from SDS-PAGE gels and subject to an in-gel trypsin digestion, to identify the peptide fragments present in the respective protein species. Fragments detected in the full-length and truncated protein samples are indicated in red on the sequences in Figure S3. In both samples, the N-terminal fragment 'RGFPGMLEVPTDGNAGLLAEPQIAMFCGR' was detected (with a single missed trypsin cleavage after the first arginine), indicating that both the full-length and truncated proteins retain their complete N-terminal sequence. In sAPPα protein samples, the C-terminal fragment

'HDSGYEVHHQ' was detected suggesting that the entire amino acid sequence is intact in this species (Figure S3a). However, the fragment closest to the C-terminus that was detected in sAPPα-tr samples was 'EQNYSDDVLANMISEPR' (Figure S3b), suggesting that this species is truncated from the C-terminal end by approximately 100 residues. This ~11 kDa section of the protein sequence corresponds to the unstructured juxtamembrane region (JMR) connecting E2 to the transmembrane domain (Figure 1) and is therefore likely susceptible to protein degradation during the expression/isolation procedure.

For additional characterisation, both samples were chemically deglycosylated by treatment with trifluoromethanesulfonic acid (TFMS) which cleaves all N- and O-linked glycosylations except the innermost N-linked GlcNAc or the innermost O-linked GalNAc, while leaving the peptide backbone intact.[11] Deglycosylation was carried out with a Glycoprofile IV Chemical Deglycosylation kit (Sigma Aldrich). Anhydrous TFMS (150 µL) with 10% anisole was added to lyophilised protein samples (~1.0 mg) and incubated for 2 hours on ice to initiate deglycosylation. Reactions were then quenched with 20 µL additions of pyridine (cooled on dry-ice) in the presence of bromophenol blue (0.2 %) until excess acid had been neutralised (as indicated by colour change). Samples were dialysed against 3×500 mL buffer (10 mM Tris, pH 8) to remove excess pyridine prior to SDS-PAGE and MS analysis (Figure S4).

After subjecting sAPPα-tr to chemical deglycosylation, SDS-PAGE reveals a small decrease in molecular weight, indicative of the removal of glycans from the protein backbone (Figure S4b). There was a significant improvement in resolution of the resulting mass spectrum (Figure S4c versus Figure S4a) which was deconvoluted to reveal a major species of approximately 57 kDa (Figure S4d), a mass ~11 kDa less than the expected MW (68.3 kDa) for the full-length protein backbone. The data supports the identification of this protein as a truncated form of the APP ectodomain including the intact N-terminus, E1, acidic and E2 domains but lacking the C-terminal JMR. Despite several

attempts to chemically deglycosylate the full-length sAPPα, a sufficiently resolved mass spectrum appropriate for mass deconvolution could not be obtained. Notably, the majority of reported glycosylation sites are located at the C-terminus of sAPPα in the JMR (Figure 1) a likely rationale for less efficient deglycosylation in sAPPα samples.

All ectodomain copper-binding studies reported in this work were performed with the full-length sAPPα.

8. Ternary Complex Isolation

Samples of reaction mixtures (~1.0 mL) containing copper (30 μM, added as $CuSO_4$), Bca (80 μM), reductant NH_2OH (1.0 mM) and selected APP proteins (30 μM each) were applied to a desalting gel filtration column (Econo-Pac 10DG packed with P6-DG gel, Bio-Rad) equilibrated in Mops buffer (50 mM, pH 7.4, 100 mM NaCl). Continued addition of buffer induced gravity flow through the resin. Elution fractions (1.0 mL) were collected and the UV-visible absorbance spectrum of each fraction was recorded. Protein fractions eluted at ~4.0 mL while small molecules (*ie* Bca) eluted at ~10.0 mL. The spectra of protein fractions are shown in Figure S6. Detected absorbance at 335 nm (corresponding to ligand Bca) in protein fractions indicates ternary complex formation. See ref [3] for further details.

9. Spectroscopic methods

UV-visible spectra were recorded on a Varian Cary 300 spectrophotometer in dual beam mode with quartz cuvettes of 1.0 cm path length. All titrations with metal ions were performed in appropriate buffers and corrected for baseline. Fluorescence emission spectra were recorded on a Varian Cary Eclipse spectrophotometer with a band pass of 20 nm for both excitation and emission. The excitation wavelength for the dansyl probes was λ = 330 nm and the emission spectra were recorded between λ

= 450-750 nm at a scale rate of λ = 600 nm min^{-1}. Circular dichroism spectra were recorded on a Chirascan-plus spectrometer (Applied Photophysics) using a 0.1 cm quartz cell. Spectra were averaged from three scans and a baseline was subtracted from each recorded spectrum.

Electron paramagnetic resonance (EPR) spectra were recorded on Bruker Elexsys E 500 EPR spectrometer. Samples of Cu^{II}-E2 and Cu^{II}-HSA were prepared by adding 0.9 equivalents Cu(II) into *apo*-proteins (each 225 μM) in an appropriate buffer (50 mM) containing 500 mM NaCl and ~10% glycerol. Samples containing both E2 and HSA were prepared by adding limiting concentrations of Cu(II) (120 μM) into a mixture of the two *apo*-proteins (150 μM each) in buffer of appropriate pH. Samples were snap-frozen in liquid nitrogen and the spectra recorded at 77 K in a liquid-nitrogen finger Dewar. EPR recording conditions: microwave frequency was in the range v = 9.446 – 9.495 GHz for all samples, but converted to a single frequency of 9.475 GHz for reporting via relationship g = 714.48 v/F, where F is the magnetic field in Gauss units, and g is the proportionality constant; microwave power 0.633 mW, modulation amplitude 4 G, sweep time 40 s, time constant 20 ms, average number of scans 30.

10. Quantification of Cu(I) binding

Cu(I) binding affinities of APP domains were quantified using the probe ligands Fs, Fz and Bca, following reported protocols.[12] Each ligand forms a chromophoric Cu(I) complex ($[Cu^{I}L_2]^{3-}$) with defined spectroscopic properties listed in Table S2. Quantification was based on the following relationships:

$$Cu^{I}L_2 + T \rightleftharpoons Cu^{I}T + 2L \tag{S1}$$

$$K_{eq} = \frac{[Cu^{I}T][L]^2}{[Cu^{I}L_2][T]} = \frac{1}{K_D \beta_2} \tag{S2}$$

$$\frac{[T]_{tot}}{[Cu^{I}]_{tot}} = 1 - \frac{[Cu^{I}L_2]}{[Cu^{I}]_{tot}} + K_D \beta_2 \left(\frac{[L]_{tot}}{[Cu^{I}L_2]} - 2\right)^2 [Cu^{I}L_2]\left(1 - \frac{[Cu^{I}L_2]}{[Cu^{I}]_{tot}}\right) \tag{S3}$$

where K_D is the conditional dissociation constant of target protein T, and β_2 is the known stepwise formation constant of the $[Cu^{I}L_2]^{3-}$ probe complex (Table S2). Cu(I) speciation was defined using absorbance data to determine equilibrium concentrations of $[Cu^{I}L_2]^{3-}$. Eqn S3 is derived from eqn S2 incorporating mass balance relationships for an effective competition described by eqn S1. Eqn S3 was used for curve-fitting of the experimental data to derive conditional dissociation constants (K'_D) for target proteins.

11. Quantification of Cu(II) binding

Cu(II) binding of APP domains and HSA were quantified using a series of fluorescent DP probes, following reported protocols.[13] These probes feature a dansyl group and emit intense fluorescence at λ_{max} ~550 nm upon excitation at ~330 nm. Each probe binds one equiv of Cu(II) with varying affinities. Cu(II) binding to probes was sensitively detected by proportional fluorescence quenching and quantified based on the following relationships:

$$Cu^{II}DP + T \rightleftharpoons Cu^{II}T + DP \quad \text{(S4)}$$

$$K_{ex} = \frac{[Cu^{II}T][DP]}{[Cu^{II}DP][T]} = \frac{K_D(Cu^{II}DP)}{K_D(Cu^{II}T)} \quad \text{(S5)}$$

$$\frac{[T]_{tot}}{[DP]_{tot}} = \frac{[Cu]_{tot} - [Cu^{II}DP]}{[DP]_{tot}} + \frac{K_D(Cu^{II}T)}{K_D(Cu^{II}DP)}\left(\frac{[Cu]_{tot}}{[Cu^{II}DP]} - 1\right)\left(1 - \frac{[Cu^{II}DP]}{[DP]_{tot}}\right) \quad \text{(S6)}$$

$$\frac{[Cu^{II}DP]}{[DP]_{tot}} = \frac{F_0 - F}{F_0 - F_1} = \frac{\Delta F}{\Delta F_1} \quad \text{(S7)}$$

where $K_D(Cu^{II}T)$ and $K_D(Cu^{II}DP)$ are the conditional dissociation constants for target and probe ligands, respectively. Eqn S6 is derived from eqn S5 incorporating the mass balance relationships for an effective competition described by eqn S4 and is a convenient format for curve-fitting of the experimental data to derive $K_D(Cu^{II}T)$ with known $K_D(Cu^{II}DP)$ (Table S2). The fluorescence intensity at 550 nm was monitored at each titration point to define Cu(II) speciation via eqn S7 where F_o, F

and F_1 are the fluorescence intensities of the DP probe upon binding 0, < 1.0 and 1.0 equiv of Cu(II), respectively. Best fits of the experimental data to eqn S6 were used to extract target dissociation constants. Reaction kinetics were fast for competition experiments between APP domains and probes DP1-3, and continuous titrations were employed in these experiments. Similar competitions between protein HSA and probes DP3 were slow to reach equilibrium, and a series of solutions were prepared and equilibrated 1-2 hours before fluorescence measurements.

Target K_D values were determined at a range of pH values in appropriate buffers (50 mM: Mes pH 5.6 – 6.7, Mops pH 6.8 – 8.1, Ches pH 8.7 – 9.2; 100 mM NaCl). The pH-dependent affinities of the Cu(II) probes DP2–4 are available (pH 6.2 – 9.2);[13] affinity characterisation of probe DP3 was extended to cover a broader pH range (5.6 – 9.2) in this work (Figure S14). The relationship between conditional affinity (K_D) and pH can be modelled using eqn S8, under conditions that (i) the Cu(II) binding site remains unchanged over the modelled pH range; and (ii) ligand compositions are known:

$$K_D = K_D^{abs}(1 + \sum_{i=1}^{n} 10^{(\Sigma_{i=1}^{n} pK_{ai} - ipH)}) \qquad \text{(S8)}$$

The conditional affinity data for APP-E2, collected from pH 5.6 – 7.4, was fitted by eqn S8, assuming n = 4 coordinating ligands with equivalent pK_a, to derive a best-fit absolute affinity (K_D^{abs}) and pK_a(His).

12. Ion mobility-mass spectrometry

Protein samples were exchanged into ammonium acetate buffer (10 mM; pH 7.4) using centrifugal filters. Cu(II) ions were added from a copper(II) acetate standard. IM-MS spectra were acquired on a Synapt HDMS system (Waters, Manchester, U.K.), using nano-ESI in the positive ion mode. Platinum-coated borosilicate capillary needles (prepared in-house) were used for sample introduction. To optimise resolution of solution relevant structures, instrument settings were modified slightly from

typical values: capillary voltage, 1.7 kV; cone voltage, 40 V; trap collision energy, 20 V; source temperature, 50 °C; backing pressure, 4 mbar; IMS cell pressure (N2), 0.4 mbar; traveling wave velocity, 300 ms^{-1}; traveling wave height, 6 V. The native MS data and drift time measurements were analysed using combined MassLynx and Driftscope software packages (Waters, Manchester, U.K., version 4.1). Extracted drift times corresponding to specific charge state ions were selected and converted to collision cross sections (CCSs) following reported protocols.[14,15] Briefly: IM-MS spectra for calibration samples (ubiquitin, myoglobin and cytochrome c; denatured conditions) were acquired and drift times of calibrant ions extracted. A nonlinear function was optimised to fit the calibration data as described in ref [14], using reference CCS values from the literature.[15] The same function was applied to samples of interest (acquired under identical machine settings to calibrant ions) to calculate CCSs for these unknowns. An estimate of the error in CCS measurement is 8−10%.[14] CCSs of model protein structures were calculated using the IMPACT projection approximation algorithm.[16] Structural coordinates used as input were obtained from the Protein Data Bank (PDB) with accession numbers indicated in the text.

13. Formal reduction potential

Formal reduction potentials were estimated from the Nernst relationship of eqn S9:

$$E\ (\mathrm{mV}) = E^0 + 59 \log\left(\frac{K_\mathrm{D}(\mathrm{Cu^{II}})}{K_\mathrm{D}(\mathrm{Cu^{I}})}\right) \qquad \text{(S9)}$$

using the relative affinities of the E2 site for Cu(I) and Cu(II) ions at pH 7.4. E^0 = 153 mV (*vs* SHE) is the standard reduction potential of Cu^{2+}/Cu^{+}.[17]

14. Catalytic aerobic oxidation of ascorbate

Reaction solutions were prepared in Mops buffer (50 mM, pH 7.4, 100 mM NaCl). Asc was added as the final component of solutions to initiate the reaction, and the change in absorbance spectrum (265 nm) was recorded for 15 mins following addition of reductant. Control solutions, prepared without Asc, were used for baseline correction. Rates were extracted from linear regions of the reaction, before Asc concentrations had become limiting.

15. Protein oxidation analysis

Samples were prepared as described in Table 4 and incubated for 1 hour before quenching reactions with excess EDTA (100 μM). Samples were then stored at 4°C prior to ESI-MS analysis, performed under denaturing conditions, as reported previously.[3]

Table S1. Properties of chromophoric Cu(I) complexes used in this work [a]

Ligand	λ_{max} of $[Cu^{I}L_2]^{3-}$ (nm)	$\varepsilon_{\lambda max}$ (cm^{-1} M^{-1})	log β_2
Fs	484	6,700	13.7
Fz	470	4,320	15.1
Bca	562	7,900	17.2
	358	42,900 [b]	

[a] Data from refs [12]. [b] With reference to equivalent copper-free Bca ligand solution (see ref [18]).

Table S2. Properties of fluorescent Cu(II) probes used in this work [a]

Probe	F_1/F_0 (550 nm)	log K_D
DP1	0.15	–8.1
DP2	0.17	–10.1
DP3	0.13	–12.3

[a] At pH 7.4; F_0 and F_1 refer to F_{550} for apo-DP and Cu^{II}-DP under identical conditions; for characterisation of probe properties at varying pH see Table 3 and Figure S14 of this work, and refs [13,19].

Table S3. Cu(II) affinities of APP domains at various pH

Protein	log K_D at given pH [a]		
	5.6	6.7	7.4
E1[b]	> –6	>8.4	> –9.4
E2	–7.9	–10.7	–11.4
sAPPα	–7.8	–10.6	–11.4

[a] Dissociation constants were determined using competition experiments with probe DP3. [b] Under identical conditions used for all experiments, E1 sites are too weak to compete effectively with probe DP3 for Cu(II) binding, and only upper affinity limit is given.

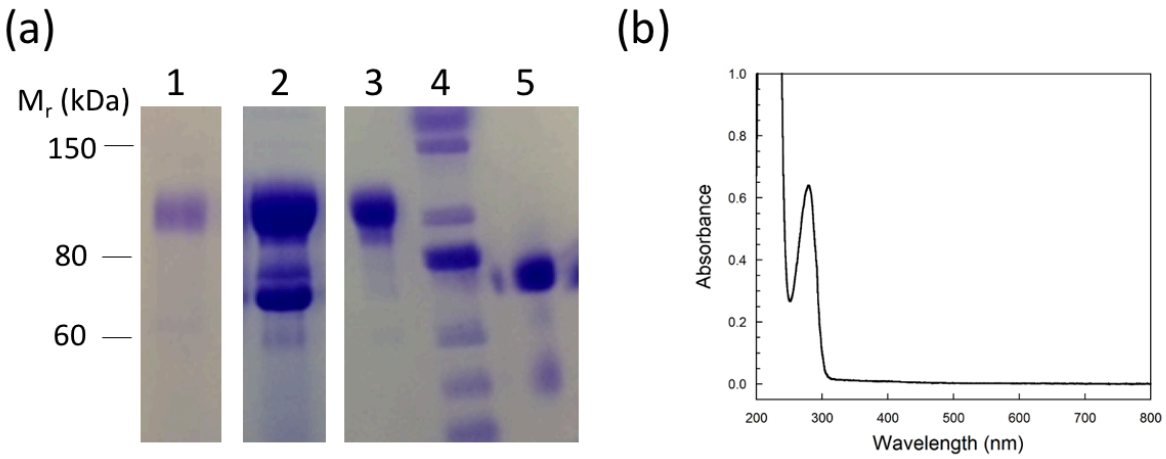

Figure S1. Purification of sAPPα from *Pichia pastoris*: (a) SDS-PAGE analysis of protein fractions during purification. Lanes: 1 supernatant, 2 elution from anion-exchange resin DE52, 3 isolated full length sAPPα, 4 protein marker, 5 isolated sAPP-tr (truncated protein) (b) UV-Visible absorbance spectra for isolated proteins (indistinguishable between sAPPα and sAPP-tr).

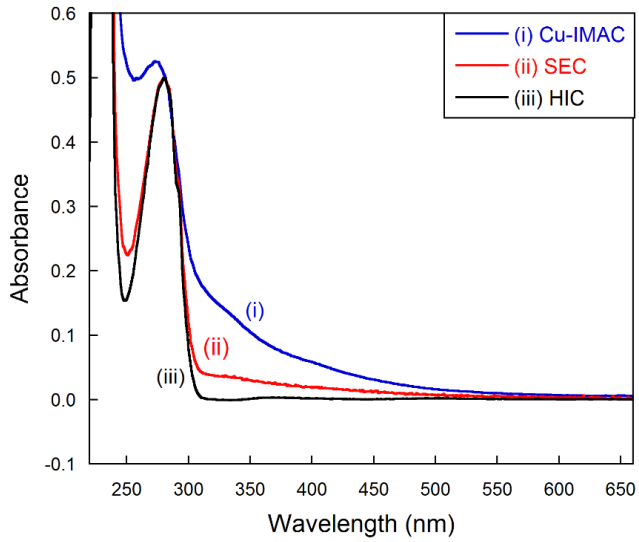

Figure S2. Representative analysis of *Pichia*-derived protein (APP-D1) at various stages of purification. UV-visible absorbance of APP-D1 elution fractions from (i) Cu-IMAC; (ii) size exclusion chromatography (SEC); (iii) hydrophobic interaction chromatography (HIC).

(a) Full-length protein

RGFPGMLEVPTDGNAGLLAEPQIAMFCGRLNMHMNVQNGKWDSDPSGTKTCIDTKEGILQYCQEVYPELQITNVV
EANQPVTIQNWCKRGRKQCKTHPHFVIPYRCLVGEFVSDALLVPDKCKFLHQERMDVCETHLHWHTVAKETCSEK
STNLHDYGMLLPCGIDKFRGVEFVCCPLAEESDNVDSADAEEDDSDVWWGGADTDYADGSEDKVVEVAEEEEVAE
VEEEEADDDEDDEDGDEVEEEAEEPYEEATERTTSIATTTTTTTESVEEVVRVPTTAASTPDAVDKYLETPGDEN
EHAHFQKAKERLEAKHRERMSQVMREWEEAERQAKNLPKADKKAVIQHFQEKVESLEQEAANERQQLVETHMARV
EAMLNDRRRLALENYITALQAVPPRPRHVFNMLKKYVRAEQKDRQHTLKHFEHVRMVDPKKAAQIRSQVMTHLRV
IYERMNQSLSLLYNVPAVAEEIQDEVDELLQKEQNYSDDVLANMISEPRISYGNDALMPSLTETKTTVELLPVNG
EFSLDDLQPWHSFGADSVPANTENEVEPVDARPAADRGLTTRPGSGLTNIKTEEISEVKMDAEFRHDSGYEVHHQ

(b) Truncated protein:

RGFPGMLEVPTDGNAGLLAEPQIAMFCGRLNMHMNVQNGKWDSDPSGTKTCIDTKEGILQYCQEVYPELQITNVV
EANQPVTIQNWCKRGRKQCKTHPHFVIPYRCLVGEFVSDALLVPDKCKFLHQERMDVCETHLHWHTVAKETCSEK
STNLHDYGMLLPCGIDKFRGVEFVCCPLAEESDNVDSADAEEDDSDVWWGGADTDYADGSEDKVVEVAEEEEVAE
VEEEEADDDEDDEDGDEVEEEAEEPYEEATERTTSIATTTTTTTESVEEVVRVPTTAASTPDAVDKYLETPGDEN
EHAHFQKAKERLEAKHRERMSQVMREWEEAERQAKNLPKADKKAVIQHFQEKVESLEQEAANERQQLVETHMARV
EAMLNDRRRLALENYITALQAVPPRPRHVFNMLKKYVRAEQKDRQHTLKHFEHVRMVDPKKAAQIRSQVMTHLRV
IYERMNQSLSLLYNVPAVAEEIQDEVDELLQKEQNYSDDVLANMISEPRISYGNDALMPSLTETKTTVELLPVNG
EFSLDDLQPWHSFGADSVPANTENEVEPVDARPAADRGLTTRPGSGLTNIKTEEISEVKMDAEFRHDSGYEVHHQ

Figure S3. Peptide fragments identified from in-gel trypsin digestion of sAPPα (a) and sAPP-tr (b) protein samples. Peptide fragments identified from tryptic digest are highlighted in red, and undetected peptides are coloured black.

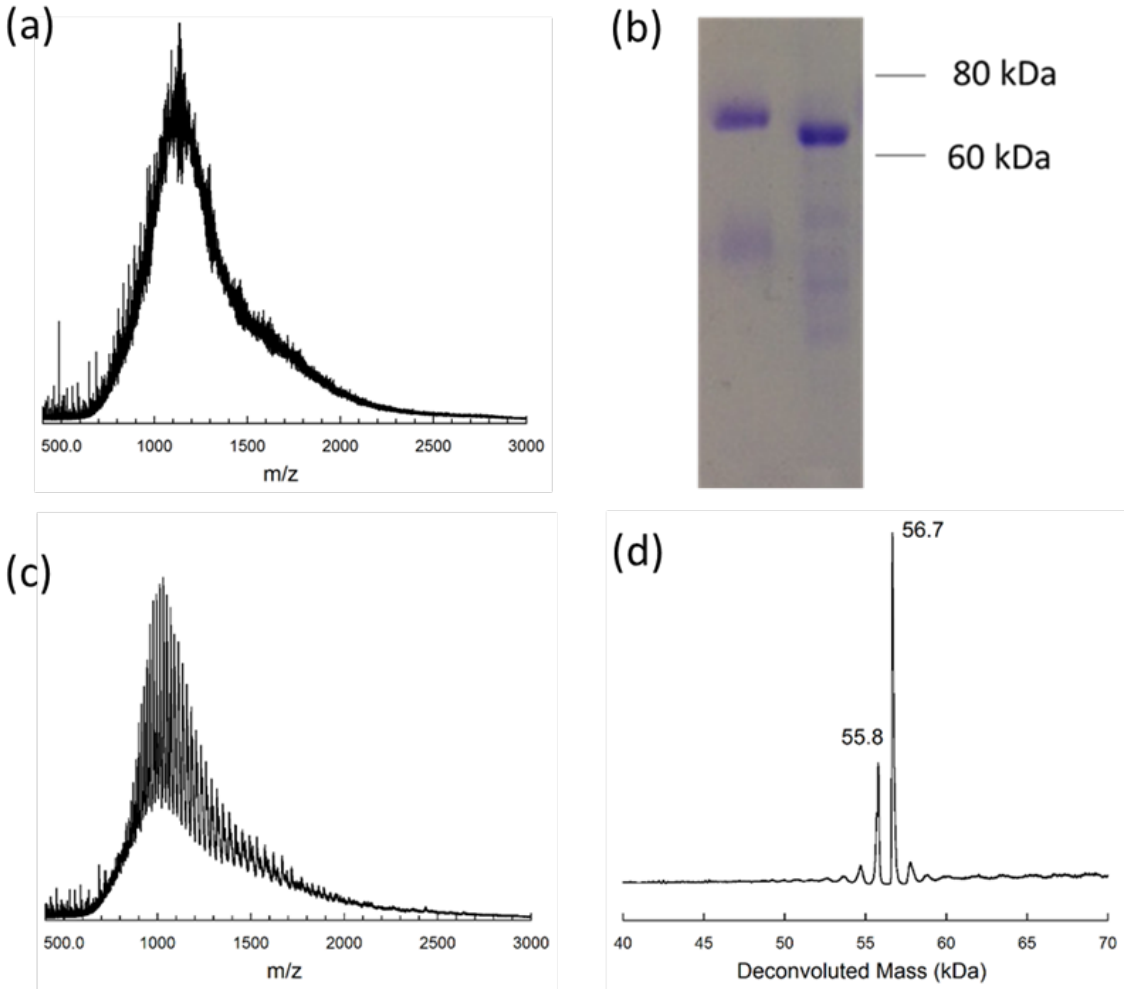

Figure S4. Analysis of truncated APP ectodomain (sAPP-tr) before and after chemical deglycosylation by treatment with trifluoromethanesulfonic acid (TFMS). (a) ESI-MS spectrum of protein before (a) and after (c) TFMS treatment. (b) SDS-PAGE shows small decrease in protein MW after TFMS treatment. (d) Deconvolution of mass spectra from (c).

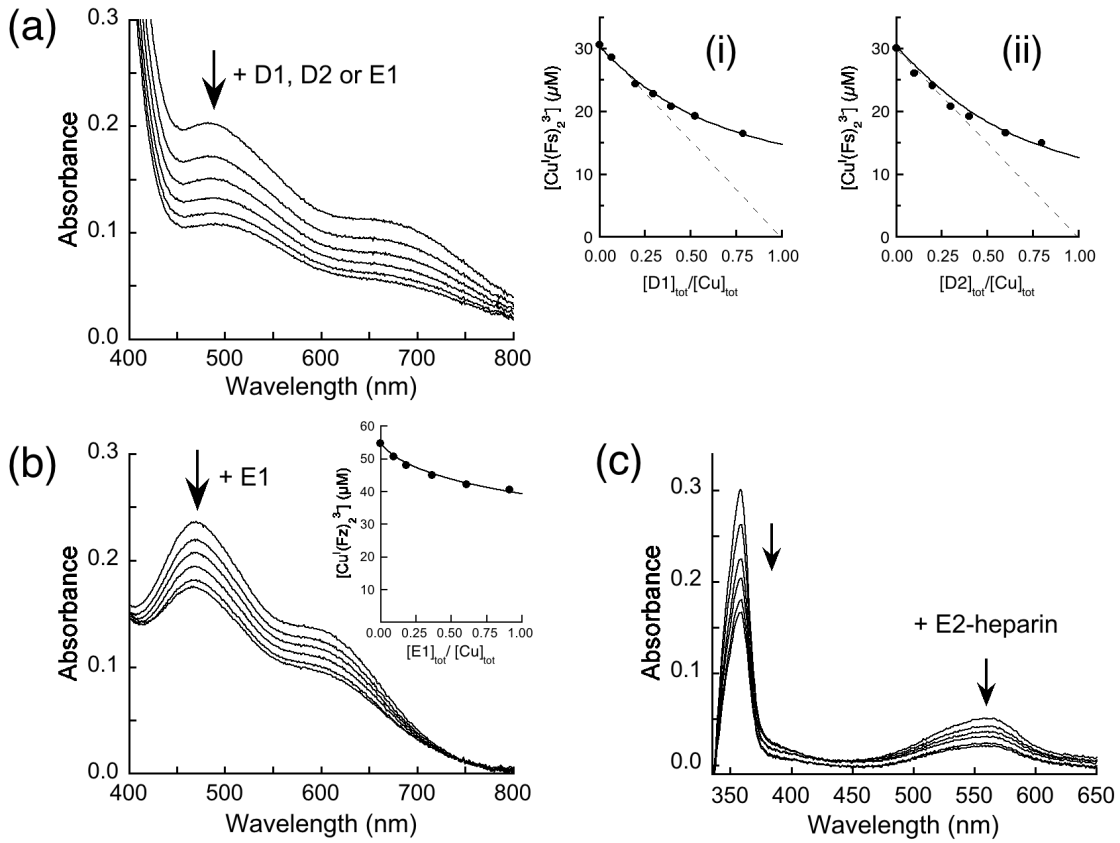

Figure S5. Quantification of Cu(I) binding affinities. Changes in solution spectra of Cu(I) chromophoric probes $[Cu^{I}L_2]^{3-}$ (L = Fs, Fz or Bca) upon titration of: (a, b) APP D1 (or D2 or E1) into a Mops solution (pH 7.4, 1.0 mM NH_2OH, 0.5 mM Asc) containing $[Cu(I)]_{tot}$ = 30.3 μM and $[Fs]_{tot}$ = 70 μM (a) or $[Cu(I)]_{tot}$ = 55 μM and $[Fz]_{tot}$ = 140 μM (b); (c) APP E2 into a Mops solution (pH 7.4, 1.0 mM NH_2OH) containing $[Cu(I)]_{tot}$ = 7.2 μM and $[Bca]_{tot}$ = 16.6 μM in the presence of one equiv of heparin H3393 (relative to protein). Shown in inset of (a) are two curve-fittings of the experimental $[Cu^{I}(Fs)_2]^{3-}$ concentrations versus the ratio of $[D1]_{tot}/[Cu]_{tot}$ (i) and $[D2]_{tot}/[Cu]_{tot}$ (ii), respectively, allowing derivation of log K_D values for APP D1 and D2 as listed in Table 2. Shown in inset of (b) is a curve-fitting of the experimental $[Cu^{I}(Fz)_2]^{3-}$ concentrations versus the ratio of $[E1]_{tot}/[Cu]_{tot}$ in solutions assuming two identical binding sites in E1, allowing derivation of an average log K_D = -10.3 for the two sites. Equivalent curve-fittings for other experiments are shown in main Figure 3.

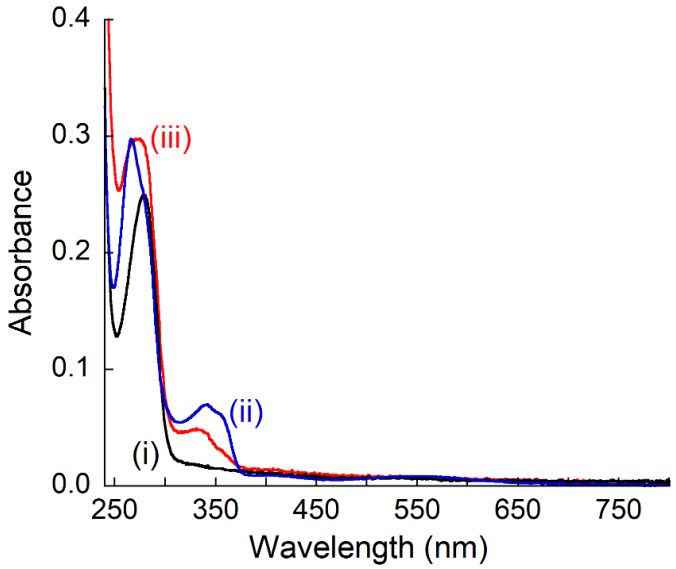

Figure S6. Solution spectra of protein fraction separated by a desalting gel-filtration column from a mixture in Mops buffer (20 mM, pH 7.4, 100 mM NaCl) containing copper (30 μM, added as $CuSO_4$), Bca (80 μM), reductant NH_2OH (1.0 mM) and selected APP protein domains (30 μM each): (i) E1, E2-qm (lacking the tetra-His M1), sAPPα plus heparin (1 eq), or pure protein; (ii) E2; and (iii) sAPPα.

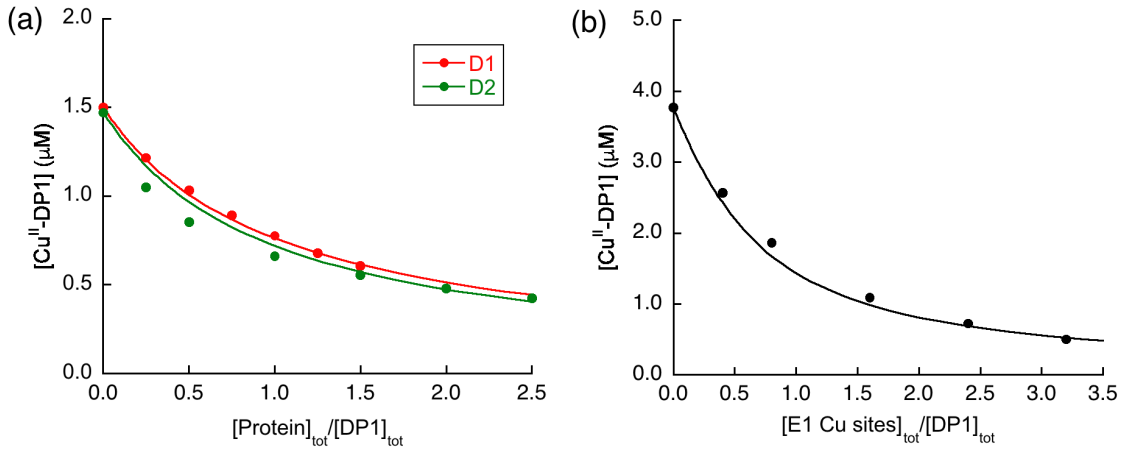

Figure S7. Quantification of Cu(II) affinities for APP domains: **(**a) D1 and D2 by titration of the respective protein into solution of Cu(II)-DP1 ($[Cu^{II}]_{tot}$ = 1.5 μM, $[DP1]_{tot}$ = 2.0 μM); and (b) E1 by titration of the protein into a solution of Cu(II)-DP1 ($[Cu^{II}]_{tot}$ = 3.8 μM, $[DP1]_{tot}$ = 5.0 μM). Solid traces are fitting of experimental data to eqn S6, assuming one or two Cu(II) sites per protein for (a) and (b), respectively. The derived log K_D values are listed in Table 2.

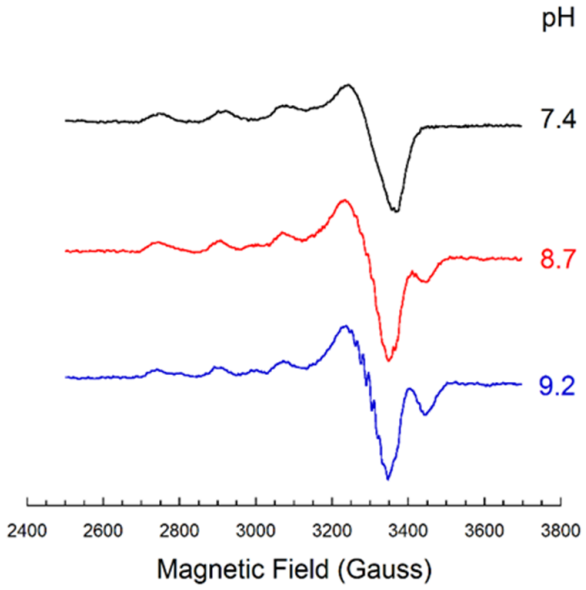

Figure S8. Frozen solution EPR spectra recorded at 77 K for Cu(II)-E2 (compositions: [Cu(II)] = 150 µM, [E2] = 200 µM in 50 mM buffer, 0.5 M NaCl) at pH 7.4 (Mops), pH 8.7 and 9.2 (Ches).

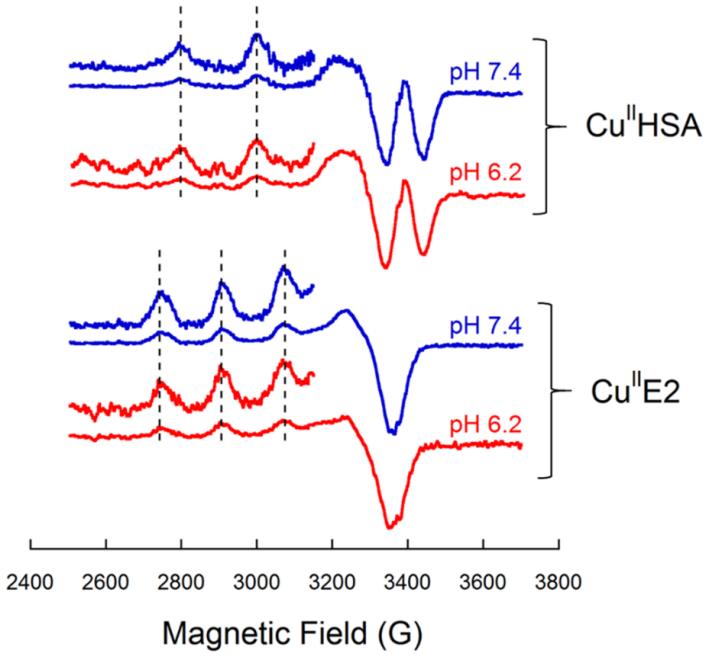

Figure S9. Frozen solution EPR spectra recorded at 77 K for the Cu(II) complexes of HSA and APP E2 (200 µM each) show consistent signals from pH 6.2 (red traces) to pH 7.4 (blue traces). Insets show enlargements of the spectra scaled up by a factor of 4. All solutions were prepared in 50 mM buffer (Mes pH 6.2; Mops pH 7.4) with 500 mM NaCl and 10 % glycerol.

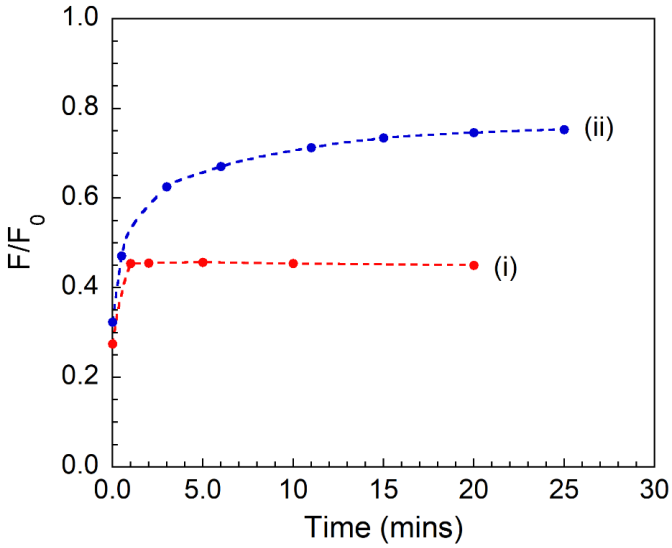

Figure S10. Kinetics of Cu(II) transfer from a solution of Cu^{II}-DP3 ($[Cu]_{tot}$ = 1.6 μM, $[DP3]_{tot}$ = 2.0 μM) to (i) APP E2 or (ii) HSA (each 2.0 μM) at pH 7.4, followed by change in fluorescence intensity at 550 nm (inversely proportional to Cu-DP3 concentration).

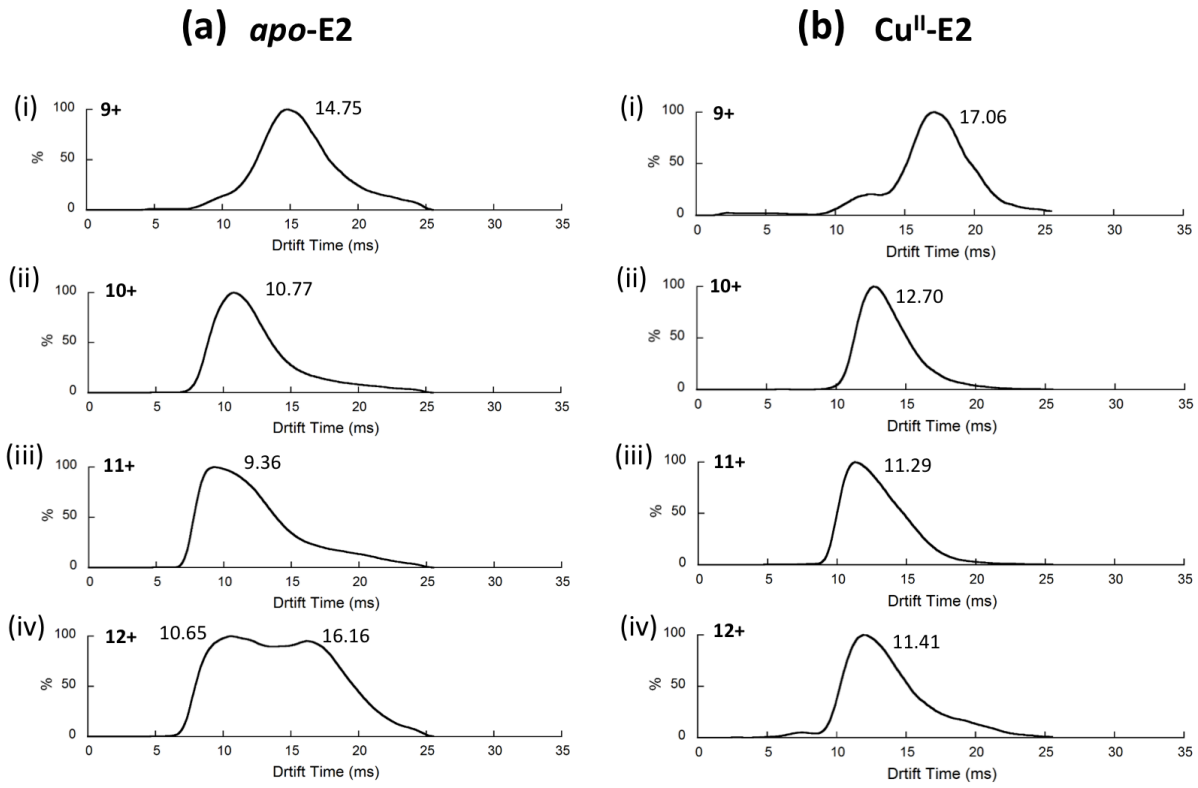

Figure S11. Arrival time distributions (ATDs) for mass-selected (a) *apo*-E2 ions; (b) Cu^{II}-bound E2 ions. Charge states are indicated: (i) 9+; (ii) 10+; (iii) 11+; (iv) 12+. All spectra were acquired under identical ion-mobility conditions. Corresponding calculated collision cross-sections (CCS) are listed in Table 3.

Note:

(1) The ATD profiles for different *apo*-E2 ions (9^+ to 12^+) were all slightly broader than their Cu^{II}-E2 counterparts (Figure S11), suggesting a higher structural flexibility of the *apo*-form. In particular, the ATD for the +12 charge *apo*-E2 ions was bimodal (Figure S11a(iv)), indicating that about half the +12 charge ions were unfolded to a certain extent. In other words, Cu(II) binding stabilizes the E2 tertiary structure.

(2) The derived CCSs for the low charge ions (9^+ and 10^+) were comparable to the theoretical values calculated from the known protein structures for *apo*- and Cu(II)-bound E2 (Table 3), confirming that these low charge ions are dominated by the folded protein forms.

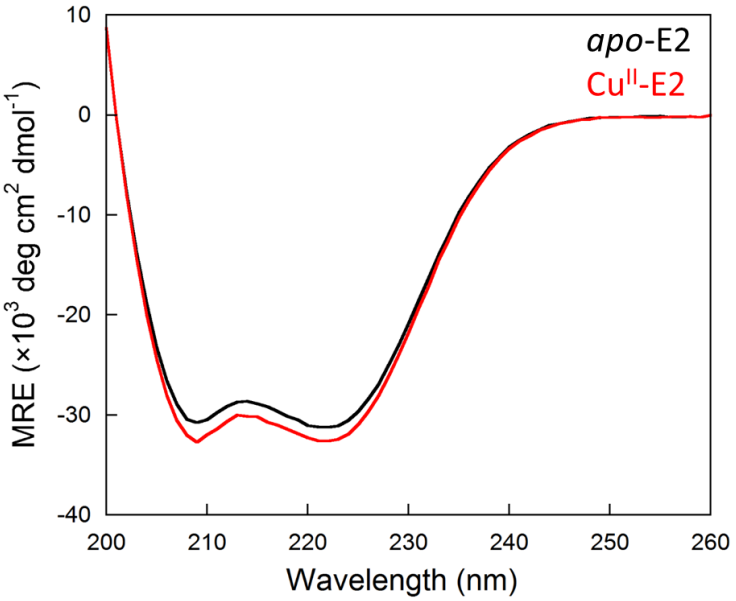

Figure S12. Circular dischroism spectra for *apo*-E2 (black trace) and Cu^{II}-E2 (red trace). Protein solutions (7.0 μM) were prepared in sodium phosphate buffer (20 mM, pH 7.4, 20 mM NaCl).

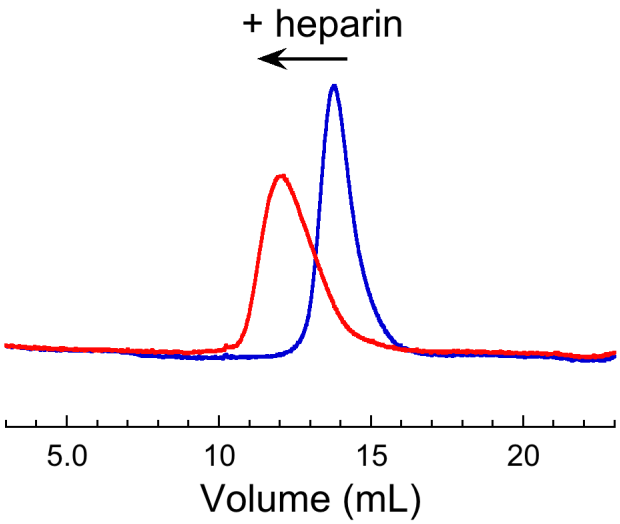

Figure S13. Size-exclusion chromotographic analysis of the isolated sAPPα in the absence (blue trace) and presence (red trace) of heparin, demonstrating that the heparin induced sAPPα dimerisation.

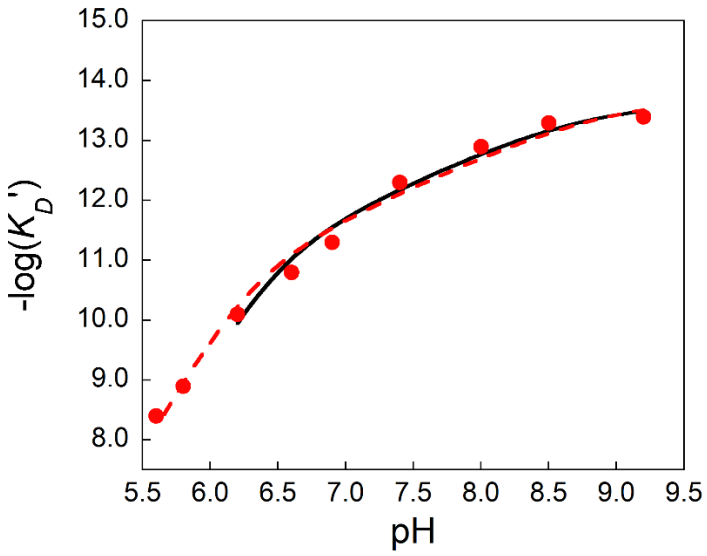

Figure S14. Extended characterisation of pH-dependent affinities of probe DP3; modelled by eqn S8 assuming a [-NH_2, 3 N^{Im} (His)] Cu(II) site. Solid black trace shows model from ref [13] covering pH 6.2-9.2; dotted red trace shows new model covering pH 5.6-9.2, deriving log K_D^{abs} = -13.7 and pK_a = 9.0 for N-ter -NH_2 and an average pK_a = 6.3 for 3 His ligands.

References

(1) Hoefgen, S., Coburger, I., Roeser, D., Schaub, Y., Dahms, S. O., and Than, M. E. (2014) Heparin induced dimerization of APP is primarily mediated by E1 and regulated by its acidic domain, *J. Struct. Biol. 187*, 30-37.

(2) Xiao, Z., Donnelly, P. S., Zimmermann, M., and Wedd, A. G. (2008) Transfer of Copper between Bis(thiosemicarbazone) Ligands and Intracellular Copper-Binding Proteins. Insights into Mechanisms of Copper Uptake and Hypoxia Selectivity, *Inorg. Chem. 47*, 4338-4347.

(3) Young, T. R., Wedd, A. G., and Xiao, Z. (2018) Evaluation of Cu(i) binding to the E2 domain of the amyloid precursor protein - a lesson in quantification of metal binding to proteins via ligand competition, *Metallomics 10*, 108-119.

(4) Calhoun, K. A., and Swartz, J. R. (2005) An Economical Method for Cell‐Free Protein Synthesis using Glucose and Nucleoside Monophosphates, *Biotechnol. Prog. 21*, 1146-1153.

(5) Henry, A., Masters, C. L., Beyreuther, K., and Cappai, R. (1997) Expression of Human Amyloid Precursor Protein Ectodomains in Pichia pastoris: Analysis of Culture Conditions, Purification, and Characterization, *Protein Expr. Purif. 10*, 283-291.

(6) Corrigan, F., Pham, C. L. L., Vink, R., Blumbergs, P. C., Masters, C. L., van den Heuvel, C., and Cappai, R. (2011) The neuroprotective domains of the amyloid precursor protein, in traumatic brain injury, are located in the two growth factor domains, *Brain Res. 1378*, 137-143.

(7) Leong, S. L., Young, T. R., Barnham, K. J., Wedd, A. G., Hinds, M. G., Xiao, Z., and Cappai, R. (2013) Quantification of Copper Binding to Amyloid Precursor Protein Domain 2 and its *Caenorhabditas elegans* Ortholog. Implications for Biological Function., *Metallomics 6*, 105-116.

(8) Duce, J. A., Ayton, S., Miller, A. A., Tsatsanis, A., Lam, L. Q., Leone, L., Corbin, J. E., Butzkueven, H., Kilpatrick, T. J., Rogers, J. T., Barnham, K. J., Finkelstein, D. I., and Bush, A. I. (2013) Amine oxidase activity of [beta]-amyloid precursor protein modulates systemic and local catecholamine levels, *Mol. Psychiatry 18*, 245-254.

(9) Cappai, R., Mok, S. S., Galatis, D., Tucker, D. F., Henry, A., Beyreuther, K., Small, D. H., and Masters, C. L. (1999) Recombinant human amyloid precursor-like protein 2 (APLP2) expressed in the yeast Pichia pastoris can stimulate neurite outgrowth, *FEBS Lett. 442*, 95-98.

(10) Shevchenko, A., Tomas, H., Havli, J., Olsen, J. V., and Mann, M. (2007) In-gel digestion for mass spectrometric characterization of proteins and proteomes, *Nat. Protoc. 1*, 2856-2860.

(11) EDGE, A. S. B. (2003) Deglycosylation of glycoproteins with trifluoromethanesulphonic acid: elucidation of molecular structure and function, *Biochem. J. 376*, 339-350.

(12) Xiao, Z., Gottschlich, L., Meulen, R. V. D., Udagedara, S. R., and Wedd, A. G. (2013) Evaluation of Quantitative Probes for Weaker Cu(I) Binding Sites Completes a Set of Four Capable of Detecting Cu(I) Affinities from Nanomolar to Attomolar, *Metallomics 5*, 501-513.

(13) Young, T. R., Wijekoon, C. J. K., Spyrou, B., Donnelly, P. S., Wedd, A. G., and Xiao, Z. (2015) A set of robust fluorescent peptide probes for quantification of Cu(ii) binding affinities in the micromolar to femtomolar range, *Metallomics 7*, 567-578.

(14) Ruotolo, B. T., Benesch, J. L. P., Sandercock, A. M., Hyung, S.-J., and Robinson, C. V. (2008) Ion mobility-mass spectrometry analysis of large protein complexes, *Nat. Protocols 3*, 1139-1152.

(15) Bush, M. F., Hall, Z., Giles, K., Hoyes, J., Robinson, C. V., and Ruotolo, B. T. (2010) Collision Cross Sections of Proteins and Their Complexes: A Calibration Framework and Database for Gas-Phase Structural Biology, *Anal. Chem. 82*, 9557-9565.

(16) Marklund, Erik G., Degiacomi, Matteo T., Robinson, Carol V., Baldwin, Andrew J., and Benesch, Justin L. P. (2015) Collision Cross Sections for Structural Proteomics, *Structure 23*, 791-799.

(17) Milazzo, G., Caroli, S., and Braun, R. D. (1978) Tables of Standard Electrode Potentials, *J. Electrochem. Soc. 125*, 261C.

(18) Xiao, Z., and Wedd, A. G. (2010) The challenges of determining metal-protein affinities, *Nat. Prod. Rep. 27*, 768-789.

(19) Yako, N., Young, T. R., Cottam Jones, J. M., Hutton, C. A., Wedd, A. G., and Xiao, Z. (2017) Copper binding and redox chemistry of the Abeta16 peptide and its variants: insights into determinants of copper-dependent reactivity, *Metallomics 9*, 278-291.